4 Extensions of the theoretical ideas

4.1 Two-time correlation functions

In some Quantum Optics problems, one needs to calculate two time correlation functions of operators A and B, such as the ones met in Section 2.3. The purpose of this section is to indicate how one can handle such a calculation with the QMC method.

4.1.1 Approach in spirit of the quantum regression theorem

To calculate a two-time expectation value such as $\langle A(t)B(t+\tau)\rangle$ by use of the QMC method, we first let a number of wave functions $|\phi\rangle$ evolve from 0 to t as explained in Section 3. We let the Schrödinger and Heisenberg pictures coincide at this time t, and for each $|\phi(t)\rangle$, we form the four new states:

$$\begin{aligned} |\chi_\pm(0)\rangle &= \frac{1}{\sqrt{\mu_\pm}}(1 \pm A^\dagger)|\phi(t)\rangle \\ |\chi'_\pm(0)\rangle &= \frac{1}{\sqrt{\mu'_\pm}}(1 \pm iA^\dagger)|\phi(t)\rangle \end{aligned} \tag{84}$$

where $\mu_\pm, \mu'_\pm$ are normalization coefficients. We then evolve the $|\chi_\pm(\tau)\rangle, |\chi'_\pm(\tau)\rangle$ according to the QMC procedure, and we calculate the four Schrödinger picture expectation values:

$$c_\pm(\tau) = \langle\chi_\pm(\tau)|B|\chi_\pm(\tau)\rangle \quad c'_\pm(\tau) = \langle\chi'_\pm(\tau)|B|\chi'_\pm(\tau)\rangle \tag{85}$$

The correlation function is now given by

$$\langle A(t)B(t+\tau)\rangle = \frac{1}{4}\Big(\mu_+\overline{c_+(\tau)} - \mu_-\overline{c_-(\tau)} + i\mu'_+\overline{c'_+(\tau)} - i\mu'_-\overline{c'_-(\tau)}\Big). \tag{86}$$

The averages, $\overline{\ \cdot\ }$, in (86) are taken both over the different outcomes for the evolution $|\chi_\pm(\tau)\rangle, |\chi'_\pm(\tau)\rangle$ between 0 and τ, and over the different outcomes for the evolution of $|\phi\rangle$ between 0 and t

The proof is in the spirit of our discussion of the Quantum Regression Theorem in Section 2.3: We show the result for one of the dyads $(|j\rangle\langle i|)(t+\tau)$, hence it follows for any operator B. Each of the four expectation values in the quantities

$$\begin{aligned} \kappa_{ij}(\tau) = \frac{1}{4} \quad & \Big(\mu_+\Big\langle\chi_+(\tau)\Big|(|j\rangle\langle i|)\Big|\chi_+(\tau)\Big\rangle - \mu_-\Big\langle\chi_-(\tau)\Big|(|j\rangle\langle i|)\Big|\chi_-(\tau)\Big\rangle \\ + \ & i\mu'_+\Big\langle\chi'_+(\tau)\Big|(|j\rangle\langle i|)\Big|\chi'_+(\tau)\Big\rangle - i\mu'_-\Big\langle\chi'_-(\tau)\Big|(|j\rangle\langle i|)\Big|\chi'_-(\tau)\Big\rangle\Big) \end{aligned} \tag{87}$$

and hence their sum, evolve as the density matrix elements ρ_{ij}, when averaged over the evolution of the $|\chi\rangle$-functions. It then follows from the Quantum Regression Theorem that these one-time averages evolve as the matrix elements $\rho_{A,ij} = \langle A(t)(|j\rangle\langle i|)(t+\tau)\rangle$.

We only need to show that the elements agree with $\rho_{A,ij}(t+\tau)$ for $\tau = 0$. This is readily verified:

$$\kappa_{ij}(0) = \frac{1}{4}\Big(\Big\langle\phi(t)|(1+A)|j\rangle\langle i|(1+A^\dagger)|\phi(t)\Big\rangle - \Big\langle\phi(t)|(1-A)|j\rangle\langle i|(1-A^\dagger)|\phi(t)\Big\rangle$$
$$+i\Big\langle\phi(t)|(1-iA)|j\rangle\langle i|(1+iA^\dagger)|\phi(t)\Big\rangle - i\Big\langle\phi(t)|(1+iA)|j\rangle\langle i|(1-iA^\dagger)|\phi(t)\Big\rangle\Big)$$
$$= \Big\langle\phi(t)|A(|j\rangle\langle i|)|\phi(t)\Big\rangle, \qquad i.e., \quad \overline{\kappa_{ij}}(0) = \rho_{A,ij}(t). \quad (88)$$

4.1.2 Example of a correlation function

The example deals with a laser driven two-level atom. We suppose that the laser is resonant so that the Hamiltonian in the rotating wave approximation can be written:

$$H_S = \frac{-\hbar\Omega}{2}(|e\rangle\langle g| + |g\rangle\langle e|) \quad (89)$$

where Ω is the Rabi-frequency characterizing the atom-laser coupling. We want to calculate the dipole correlation function:

$$C(t,\tau) = \langle(|e\rangle\langle g|)(t)(|g\rangle\langle e|)(t+\tau)\rangle. \quad (90)$$

This calculation is performed in steady state, so that the Fourier transform gives access to the fluorescence spectrum. Starting at time $t = 0$ in the ground state, we let the states evolve for a time sufficiently long to obtain several quantum jumps (spontaneous emission events). Within a density matrix description, this guarantees that the steady state has been reached. In the QMC approach, it implies that there is no memory of initial conditions. From each $|\phi(t)\rangle$ obtained in this way, we generate two pairs of states $|\chi_\pm(\tau)\rangle$ and $|\chi'_\pm(\tau)\rangle$ as defined above, and we calculate the average of the quantities (85,86). The results of this procedure are indicated in Fig. 8, where we show the values of $C(t,\tau)$ normalized to its value at $\tau = 0$ in comparison with the analytic predictions [26]. $n = 500$ wavefunctions are applied in the simulation.

4.1.3 The Spectrum as a one-time average (II)

A wave function simulation of the spectrum, different from the one discussed above, may be formulated along the ideas of Section 2.3.4. One has to simulate the situation described in terms of density matrices, i.e. use a wave function of the type [8]

$$|\psi\rangle = |\phi\rangle \otimes |0_\omega\rangle + |\phi_\omega\rangle \otimes |1_\omega\rangle, \quad (91)$$

and then determine the norm of the second part of this function. This function is *not* equivalent to the one in Eq.(12). With the single field mode of interest incorporated

[8] Mollow [44] actually showed, in this spirit, how the spectrum can be calculated as a one-time average.

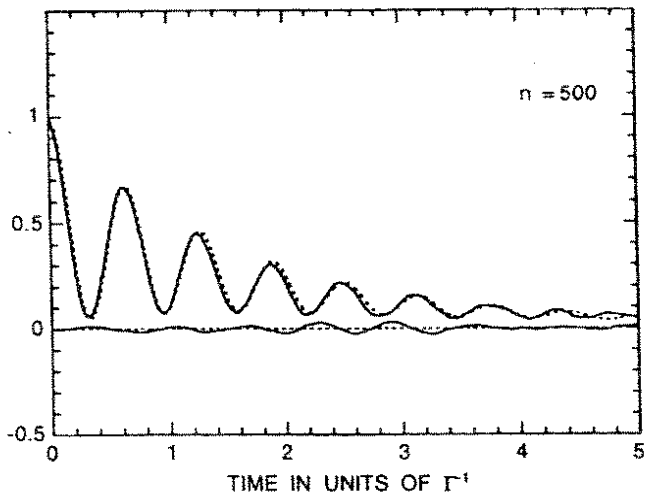

Figure 8: *In solid lines, real part (upper curve) and imaginary part of the dipole correlation function for a two-level atom* $\langle(|e\rangle\langle g|)(t)(|g\rangle\langle e|)(t+\tau)\rangle / \langle(|e\rangle\langle e|(t)\rangle$. *In dotted lines, we have indicated the exact result obtained from the Optical Bloch Equations and the Quantum Regression theorem. The field parameters are* $\Omega = 10\Gamma, \delta = 0$, *so that a Fourier transform of the results should yield the spectrum in Fig.2.*

in the system S, the function in (91) is rather the zero-*reservoir-photon* part of (12), and our simulation scheme works by evolving such a function in time. Due to the weak coupling the norm of the wavefunction resides mostly in the zero-*cavity-photon* component of (91), hence the system jumps (caused by $\sqrt{\Gamma}|g\rangle\langle e|$ in case of the two-level atom) are decided by this component, but they affect both. Since the coupling is weak the component $|\phi_\omega\rangle$ depends on $|\phi\rangle$ but not the other way round. These ideas have been developed further in [45, 46] to identify other spectral properties, and to make efficient numerical schemes.

The method is certainly more intuitive than the QRT-based approach. It is not clear, however, if it is also more efficient from a numerical point of view: with this method an auxiliary wave function $|\phi_\omega\rangle$ has to be propagated in time for *each* frequency component in the spectrum, whereas the approach in Section 4.1.2 only evolves one set of functions, and then applies a Fourier transform. In addition, whereas the two-time average, like in (21), is quite standard in a number of problems, some creativity may be required to identify the corresponding physical one-time average and to identify equations that are not more complicated than the ones of the QRT approach. For another example see e.g. the discussions of momentum diffusion in laser cooling [34, 35].

The most extensive calculation of a spectrum, and probably the best agreement ever obtained in the confrontation of laser cooling theory and experiment was published recently. In Fig.9 the measured fluorescence spectrum from a sample of Cs atoms, cooled in one dimension to a regime where the external motion has to be described quantum mechanically [47], is compared with a calculation by Marte *et al* [48]. The lines in the spectrum indicate the Bohr-frequencies between levels of external motion in the light-induced potential. The calculations are probably at the limit of problems

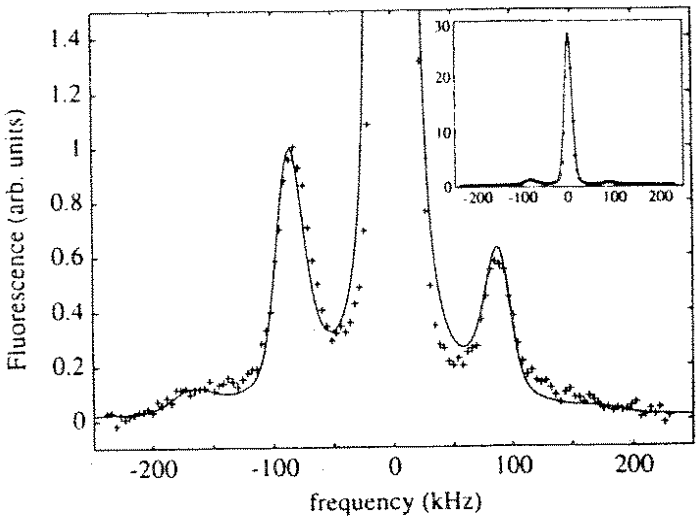

Figure 9: *Spectrum of resonance fluorescence as a function of the frequency difference to the exciting laser. The solid line is the theoretical spectrum convoluted with a Lorentzian corresponding to the finite detector bandwidth and a residual Doppler broadening due to the motion in the non-cooled direction perpendicular to the cooling laser, and nearly perpendicular to the direction of observation. Crosses are experimental results.*

that can be treated by density matrices.

4.2 Equivalent QMC simulations for a given master equation

It is a general result that the Monte-Carlo evolution outlined above represents a possible history of the system wave function in the presence of a suitable continuous detection process [3, 6]. In order to get some physical understanding of the simulation, it may therefore be useful, to refer to such a continuous detection process, as if it were really performed. In general one may device several different and mutually incompatible detection processes for the evolution of a given quantum system. This corresponds to the application of various sets of C_m's, each associated with a certain detection scheme, and these sets may be related by suitable linear combinations. The relaxation equation (56,57) must of course remain the same for every detection scheme simulated, but the evolution of the individual Monte Carlo Wave Functions may be very sensitive to the choice [4]. We discuss in this section the existence of several different Monte-Carlo approaches for a given relaxation operator $\mathcal{L}_{\mathbf{relax}}$, leading on average to the same results, but with very different physical pictures.

Here we restrict ourselves to a class of Monte-Carlo approaches which are related by an invariance property of the relaxation operator $\mathcal{L}_{\mathbf{relax}}$ in Eq.(57). Suppose that

there exists a unitary operator T, acting in the Hilbert space of the system, such that:

$$T\left(\mathcal{L}_{\text{relax}}(\rho_S)\right)T^\dagger = \mathcal{L}_{\text{relax}}(T\rho_S T^\dagger). \tag{92}$$

The operator T can for instance be a rotation operator and (92) is then fulfilled if the dissipation process is isotropic. Eq.(92) can be transformed into:

$$\mathcal{L}_{\text{relax}}(\rho_S) = T^\dagger\ \mathcal{L}_{\text{relax}}(T\rho_S T^\dagger)\ T \tag{93}$$

and the relaxation operator can also be written as:

$$\mathcal{L}_{\text{relax}}(\rho_S) = -\frac{1}{2}\sum_m \left(D_m^\dagger D_m \rho_S + \rho_S D_m^\dagger D_m\right) + \sum_m D_m \rho_S D_m^\dagger \tag{94}$$

with

$$D_m = T^\dagger C_m T. \tag{95}$$

We can therefore perform the Monte-Carlo simulation either with the set of operators C_m or with the set of operators D_m. The physical pictures given by these two Monte-Carlo simulations may be very different, although their predictions concerning operator averages are the same.

4.2.1 Spontaneous emission with Zeeman degeneracy

We can illustrate this by spontaneous emission from a two-level atom, where we take into account the angular momentum of the ground (J_g) and excited (J_e) levels. In order to give the relaxation operator a simple form, we write it in the $|J_g, m_g\rangle_z, |J_e, m_e\rangle_z$ basis, referred to a quantization axis z,

$$\mathcal{L}_{\text{relax}}(\rho_S) = -\frac{\Gamma}{2}\left(P_e\rho_S + \rho_S P_e\right) + \Gamma\sum_q (\vec{\epsilon}_q{}^*.\vec{S}^-)\rho_S(\vec{\epsilon}_q.\vec{S}^+) \tag{96}$$

Here, P_e is the projection operator on the excited state manifold, $P_e = \sum_{m_e} |J_e, m_e\rangle\langle J_e, m_e|$. $\vec{\epsilon}_q$ is the standard spherical basis associated with the $z$axis: $\vec{\epsilon}_\pm = \mp\frac{1}{\sqrt{2}}(\vec{u}_x \pm i\vec{u}_y)$, $\vec{\epsilon}_0 = \vec{u}_z$, and $\vec{S}^+$ and $\vec{S}^-$ are raising and lowering operators proportional to the atomic dipole operator:

$$\begin{cases} \vec{\epsilon}_q \cdot \vec{S}^+ |J_g, m_g\rangle_z = \langle J_g\ m_g\ 1\ q | J_e\ m_e = m_g + q\rangle |J_e, m_e = m_g + q\rangle_z \\ \vec{\epsilon}_q \cdot \vec{S}^+ |J_e, m_e\rangle_z = 0 \\ \vec{\epsilon}_q{}^* \cdot \vec{S}^- = \left(\vec{\epsilon}_q.\vec{S}^+\right)^\dagger \end{cases} \tag{97}$$

A Clebsch-Gordan coefficient enters in the coupling of the ground and excited state sublevels. The QMC procedure involves three operators:

$$C_q = \sqrt{\Gamma}\left(\vec{\epsilon}_q{}^* \cdot \vec{S}^-\right) \quad q = 0, \pm 1, \tag{98}$$

and we note that the relation

$$\sum_{q=-1}^{1} C_q^\dagger C_q = \Gamma \, \vec{S}^+ \cdot \vec{S}^- = \Gamma \, P_e \tag{99}$$

ensures that the relaxation operator (96) indeed has the same structure as (57). From the measurement point of view presented in Section 3.2, the branching corresponds to a simulation where not only the number of photons emitted during δt is detected, but also the angular momentum of those photons along a given axis z.

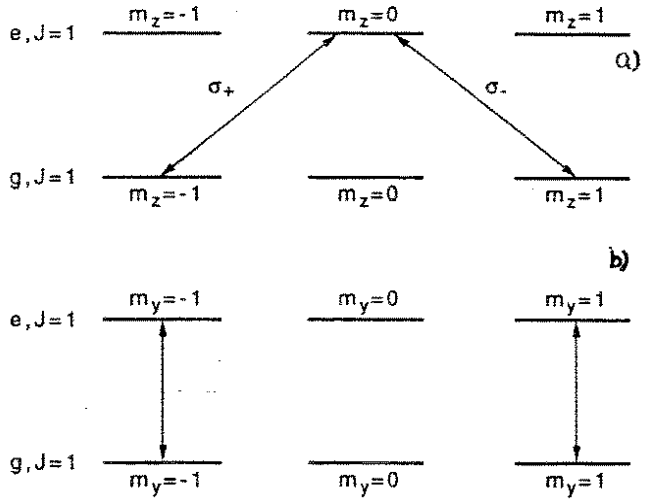

Figure 10: *Level scheme of a $J_g = 1 \; - \; J_e = 1$ atomic transition, induced by two waves with σ^+ and σ^- polarization with respect to the z axis. (a) A certain linear combination of the two ground states with $m_z = \pm 1$ will be non-absorbing, (b) if the y axis is used for quantization in a point in space where the total electric field vector is in the y direction, the non-absorbing ground state is simply the $m_y = 0$ state (because the Clebsch-Gordan coefficient $\langle 1010|10\rangle$ vanishes).*

4.2.2 Example: evolution towards a dark state

It is in principle straightforward to write the master equation with the spherical components defined with respect to any axis, and to perform the simulation with the corresponding transformed operators D_q. We give an example of two equivalent Monte-Carlo simulations for the same physical process. Consider a $J_g = 1 \leftrightarrow J_e = 1$ transition induced by two resonant laser fields with the same intensity and polarizations σ_+ and σ_- with respect to the z axis (Fig. 10a). It is known from the analysis by Optical Bloch Equations that the atomic population is eventually trapped in a ground state which is not coupled to the laser field. This is related to the "dark resonance" phenomenon [49]. If the two waves are in phase, this "dark" state is:

$$|\phi_{NC}\rangle = (|g, m_z = -1\rangle + |g, m_z = 1\rangle)/\sqrt{2} \tag{100}$$

The first QMC analysis can be performed using the operators C_q defined in (98). Suppose that the atom starts in $|g, m_z = -1\rangle$. The atom-laser coupling leads first to

an increase of the population of the excited state $|e, m_z = 0\rangle$. A spontaneous photon may then be emitted (Fig.11a) and, depending on its angular momentum $q_z = \pm 1$, this process puts the atom into $|g, m_z = \mp 1\rangle$ (the transition $|e, m_z = 0\rangle \rightarrow |g, m_z = 0\rangle$ is forbidden due to the vanishing Clebsch-Gordan coefficient). But, it may also happen that, even after a very long time, no spontaneous photon has been detected; the successive steps "evolution due to the non-hermitian Hamiltonian H, renormalization of the resulting wavefunction" cause a continuous rotation from $|g, m_z = \pm 1\rangle$ into $|\phi_{NC}\rangle$, and trapping in this state has occured (last part of the time sequence of Fig. 11a). Note that the continuous rotation, which is the only possible way for the system to enter the trapping state, is of the same type as the one met in Section 3.2 for the spontaneous decay of a two-level atom in a superposition of the ground and excited state.

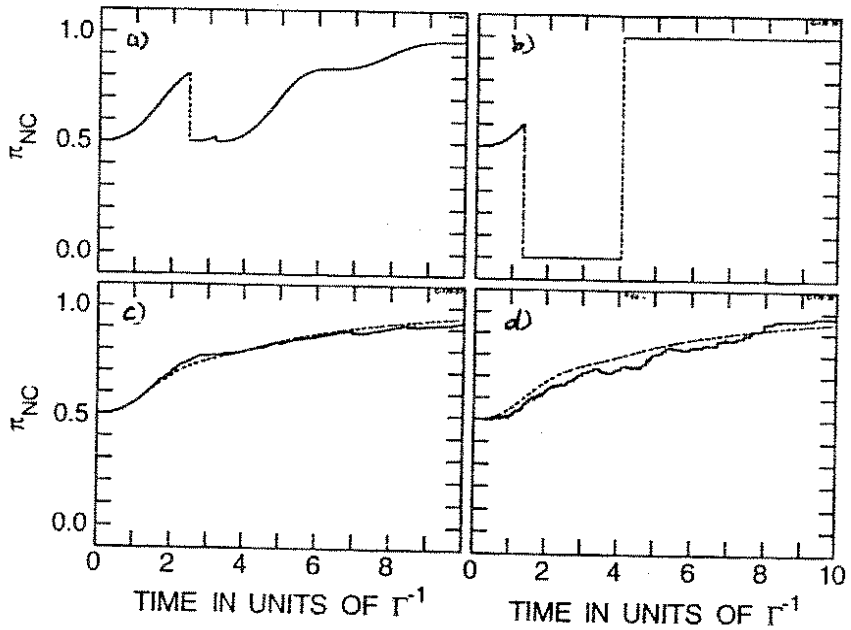

Figure 11: *Simulations of evolution towards the dark state with two different measurement schemes, single trajectories are shown in part a) and b), and averages over 100 MCWF's are shown in part c) and d) of the figure.*

Now, we replace the set of operators C_q by a different set obtained by choosing a different quantization axis. For instance, suppose that we choose this new quantization axis y parallel to the resulting linear polarization of the laser light at the atom position. Because of the "π polarization" of the laser light along that axis (see Fig.10b), we now identify the trapping state as

$$|\phi_{NC}\rangle = |g, m_y = 0\rangle \tag{101}$$

and we perform the Monte-Carlo simulation using the set of operators D_q analogous to those given in (98), but defined now with respect to the y axis. In Fig. 11b we have illustrated such a simulation involving two quantum jumps. We start again in the state $|g, m_z = -1\rangle$ which we now expand in the $|g, m_y\rangle$ basis. During the first

part of the evolution, a continuous rotation towards $|g, m_y = 0\rangle$ takes place. Then a first photon with $q_y = 0$ is detected; this detection projects the wave function onto a superposition of $|g, m_y = \pm 1\rangle$ and the population of the trapping state $|g, m_y = 0\rangle$ is 0. The atom then cycles between $|g, m_y = \pm 1\rangle$ and $|e, m_y = \pm 1\rangle$, and the population of the trapping state remains zero until one detects a second photon with a polarization $q_y = \pm 1$. This detection projects the wave function into the trapping state. The way the system enters the dark state is here *discontinuous*, and it may be more readily understood as a kind of optical pumping.

We check in Figs.11c and 11d that the two simulations lead to the same average results. We observe smaller fluctuations in the results obtained with the quantization along the z axis; the reason for this difference in the "quality" of the simulation is that $|\phi_{NC}\rangle\langle\phi_{NC}|$ is "more local" (in the sense of Eq.(74)) in the y basis than in the z basis.

4.3 QMC and continuous stochastic equations

4.3.1 "Homodyne and heterodyne jumps"

Carmichael has shown that for the particular case of homodyne detection of the fluorescence light, the quantum jump formalism can be transformed into a *continuous* stochastic equation [6]. Actually his proof can be extended to the most general case [5, 50]: The first step is to write the relaxation operator $\mathcal{L}_{\text{relax}}$ as:

$$\mathcal{L}_{\text{relax}}(\rho_S) = -\frac{1}{2}\sum_{m,\varepsilon}\left(D^\dagger_{m,\varepsilon}D_{m,\varepsilon}\ \rho_S + \rho_S\ D^\dagger_{m,\varepsilon}D_{m,\varepsilon}\right) + \sum_{m,\varepsilon} D_{m,\varepsilon}\ \rho_S\ D^\dagger_{m,\varepsilon} \tag{102}$$

where $\varepsilon = \pm 1$ and where the $D_{m,\varepsilon}$ are defined as:

$$D_{m,\varepsilon} = \frac{\mu \mathbb{1} + \varepsilon C_m}{\sqrt{2}} \tag{103}$$

One easily shows that $\mathcal{L}_{\text{relax}}$ in (102) is identical with the one in (57). The coefficient μ is arbitrary at this stage; μ^2 has the dimension of inverse time, and we just require in the following $\mu^2 \gg |\eta|$, where $\hbar\eta$ is a typical eigenvalue of H_S (for the two-level atom case, $\eta \sim \Gamma, \Omega, \delta$). We now perform a Monte-Carlo evolution of the wave function, using the set of operators $D_{m,\varepsilon}$. Because of the large magnitude of μ^2, this simulation with the $D_{m,\varepsilon}$ operators involves a much larger number of quantum jumps in a given time interval Δt than a simulation with the C_m's. But the change of the wave function in a given quantum jump:

$$|\phi\rangle \longrightarrow \frac{D_{m,\varepsilon}|\phi\rangle}{\|D_{m,\varepsilon}|\phi\rangle\|} \tag{104}$$

is correspondingly much smaller since $D_{m,\varepsilon}$ is nearly proportional to the identity operator $\mathbb{1}$. In the limit of very large μ, the Monte-Carlo evolution of the wave function therefore tends towards a continuous stochastic evolution. In Carmichael's homodyne detection problem, the form (103) for the $D_{m,\varepsilon}$ has a clear interpretation. These jump

operators correspond to the detection of a photon after one has mixed the light emitted by the system with a local oscillator field. The parts in $\mu\mathbb{1}$ and C_m correspond to the field originating from the local oscillator and the field emitted by the atom, respectively, see Fig 12. The condition $\mu^2 \gg |\eta|$ ensures that the intensity of the local oscillator is much higher than the intensity of the light emitted by the atom, as always in homodyne detection.

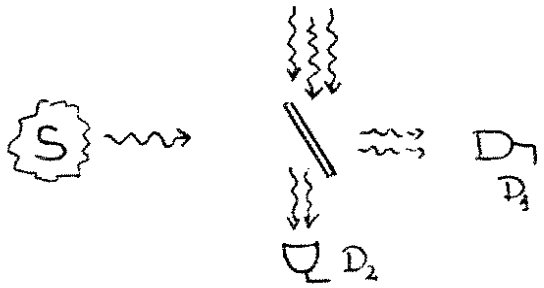

Figure 12: *Homodyne detection of fluorescence light. The radiation, emitted by the source S, is mixed on a beam splitter with a classical local oscillator field and detected by the two photon detectors D_1 and D_2.*

We now choose a time interval Δt such that

$$\mu^{-2} \ll \Delta t \ll |\eta|^{-1} \,. \tag{105}$$

This implies that the number of jumps $N_{m,\varepsilon}$ occurring with a given operator $D_{m,\varepsilon}$ during Δt will be large compared to 1 since $\mu^2\ \Delta t \gg 1$, but at the same time we obtain only a small change in the system wave function since $|\eta|\Delta t \ll 1$. The operator $\mathcal{O}$ describing the action of all the jumps occuring during Δt is a product of the various $D_{m,\varepsilon}$ and, to first order in $\sqrt{\Delta t\ |\eta|}$, it can be approximated to

$$\mathcal{O} \simeq \left(\frac{\mu}{\sqrt{2}}\right)^N \left(\mathbb{1} + \frac{1}{\mu}\sum_m (N_{m,+} - N_{m,-})\ C_m\right) \tag{106}$$

where $N = \sum_{m,\varepsilon} N_{m,\varepsilon}$ is the total number of jumps occurring during Δt. The wave function at time $t + \Delta t$ can now be written before normalization:

$$|\phi(t+\Delta t)\rangle = \left(\mathbb{1} + \frac{1}{i\hbar}H_S\Delta t - \frac{1}{2}\Delta t\sum_m C_m^\dagger C_m + \sum_m \frac{N_{m,+} - N_{m,-}}{\mu} C_m\right)|\phi(t)\rangle \tag{107}$$

where we have taken into account both the non-hermitian evolution during Δt and the effect of the multiple quantum jumps. The numbers $N_{m,\varepsilon}$ are Poissonian random variables, and based on expressions analogous to Eq.(62), we obtain for the average values and standard deviations:

$$\overline{N_{m,\varepsilon}} \ \simeq\ \frac{\mu^2\Delta t}{2}\left(1 + \frac{\varepsilon}{\mu}\langle C_m + C_m^\dagger\rangle\right)$$

$$\Delta N_{m,\epsilon} \simeq \frac{\mu}{\sqrt{2}}\sqrt{\Delta t}, \tag{108}$$

where the average value $\langle C_m + C_m^\dagger \rangle$ is taken in $|\phi(t)\rangle$. In the limit of large $N_{m,\epsilon}$, we can then approximate the random variable $N_{m,+} - N_{m,-}$ appearing in (107) by:

$$\frac{N_{m,+} - N_{m,-}}{\mu} = \Delta t \langle C_m + C_m^\dagger \rangle + \Delta\zeta_m \tag{109}$$

where $\Delta\zeta_m$ is a real gaussian random variable with zero mean and a standard deviation equal to $\sqrt{\Delta t}$. Finally we normalize the wave function (107) and we obtain:

$$\begin{aligned} |\Delta\phi\rangle = & \frac{1}{i\hbar} H_S |\phi(t)\rangle \, \Delta t \\ & + \frac{1}{2}\sum_m \left(\langle C_m + C_m^\dagger \rangle C_m - C_m^\dagger C_m - \frac{1}{4}\langle C_m + C_m^\dagger \rangle^2 \right) |\phi(t)\rangle \Delta t \\ & + \frac{1}{2}\sum_m \left(2C_m - \langle C_m + C_m^\dagger \rangle \right) |\phi(t)\rangle \Delta\zeta_m \, . \end{aligned} \tag{110}$$

In (110), we have kept terms linear in $\Delta\zeta_m$ and Δt, and we have replaced all the quadratic terms $\Delta\zeta_m \Delta\zeta_{m'}$ by their mean $\Delta t \, \delta_{m,m'}$. In the limit $\mu \to +\infty$, $\Delta t \to 0$, this equation can be interpreted as an Itô stochastic equation.

Another class of stochastic equations for system wave functions, which is also equivalent to the master equation, has been introduced in quantum optics by Gisin and Percival [11, 12]. Their complex Itô stochastic process is given by:

$$\begin{aligned} |\Delta\phi\rangle = \frac{1}{i\hbar} H_S |\phi\rangle \Delta t \; & + \; \sum_m \left(\langle C_m^\dagger \rangle C_m - \frac{1}{2} C_m^\dagger C_m - \frac{1}{2}\langle C_m^\dagger \rangle \langle C_m \rangle \right) |\phi\rangle \Delta t \\ & + \; \sum_m \left(C_m - \langle C_m \rangle \right) |\phi\rangle \, \frac{\Delta\xi_m}{\sqrt{2}} \end{aligned} \tag{111}$$

where $\langle C_m \rangle = \langle \phi | C_m | \phi \rangle$, and where the $\Delta\xi_m$ are independent complex Wiener processes [51].

In Fig.13 is shown an example of a simulation of continuous stochastic type for a driven damped harmonic oscillator, which may represent a cavity field mode [12]. In the simulation all 5 wave functions are taken initially in the $n = 8$ number state, and via different trajectories they approach the stationary solution, which is a pure, coherent, state of the oscillator. The figure shows the mean value of n for each of the 5 wave functions.

The evolution given by Eq.(111) corresponds to a simulation of a heterodyne detection of the fluorescence signal from an atom. The set-up for such a detection is like in Fig.12, but the frequency of the local oscillator is different from that of the laser driving the atomic transition $|g\rangle \to |e\rangle$. Imagine that the coefficient μ in (105) rotates in the complex plane as a function of time, corresponding to a time dependent phase between the local oscillator and the system dipole. This leads to a complex process

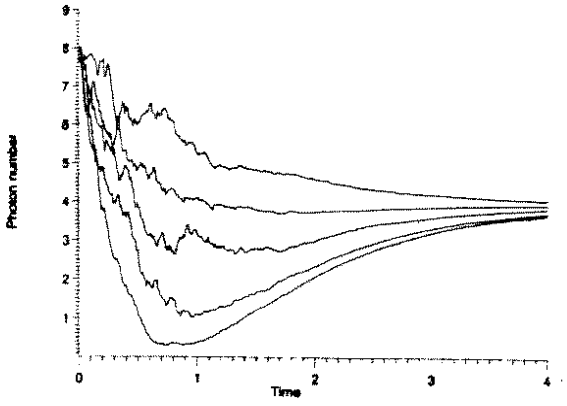

Figure 13: *Mean photon number in five different field states, evolved according to (111). The system is a driven and damped cavity field mode, converging from the initial $n = 8$ photon number state towards a pure coherent state.*

as the one in Eq.(111). The heterodyne simulation seems more "unique" than the homodyne simulation since one has to specify the oscillator/dipole phase difference in the latter case. This uniqueness property is shared with the jump evolution of Section 3, but it is not evident that it is physically meaningful to focus on this property. The wavefunctions given by (63,64),(110) or (111) are all as much, or as little, meaningful if no detection is made.

4.3.2 Geometric pictures

In case of the two-level atom, the density matrix can be represented geometrically by the Bloch vector. With the notation of [50]

$$\begin{pmatrix} x \\ y \\ z \end{pmatrix} \equiv \begin{pmatrix} \Big\langle (|e\rangle\langle g| + |g\rangle\langle e|) \Big\rangle \\ -i\Big\langle (|e\rangle\langle g| - |g\rangle\langle e|) \Big\rangle \\ \Big\langle (|e\rangle\langle e| - |g\rangle\langle g|) \Big\rangle \end{pmatrix} = r \begin{pmatrix} \sin\theta\cos\phi \\ \sin\theta\sin\phi \\ \cos\theta \end{pmatrix}. \tag{112}$$

For a pure state, $r^2 = x^2 + y^2 + z^2$ equals unity, but for the more general density matrices, the vector is always inside the unit sphere. The simulation schemes can now be viewed as ways of obtaining the evolution of this vector inside the unit sphere as the average of pure states, i.e. vectors on the surface of the sphere. In Fig.14 are shown the positions (i.e. the values of $\cos\theta$ and ϕ in (112)) for 20.000 state vectors. The three plots from [50] correspond to a) homodyne detection with a local oscillator in phase with the driving laser field b) homodyne detection with a phase difference of $\pi/2$ and c) heterodyne detection. All calculations are made with a vanishing laser detuning, $\delta = 0$ and with $\Omega = 7\sqrt{2}\Gamma$. For these parameters the stationary state Bloch vector has $r \simeq 0.1, \cos\theta \simeq -0.2$ (below the equator) and $\phi = \pi/2$, which should be the average of the 20.000 points shown in each figure. A fourth plot, corresponding to the jump

evolution described in Sec. 3.2.1 would have all points spread out on the $\phi = \pm\pi/2$ great circle, with more than half of the points on the $\phi = +\pi/2$-side, since after each jump, or complete oscillation, the atom is in the ground state, i.e. the Bloch vector is on the south pole, and the evolution proceeds this way around the Bloch sphere.

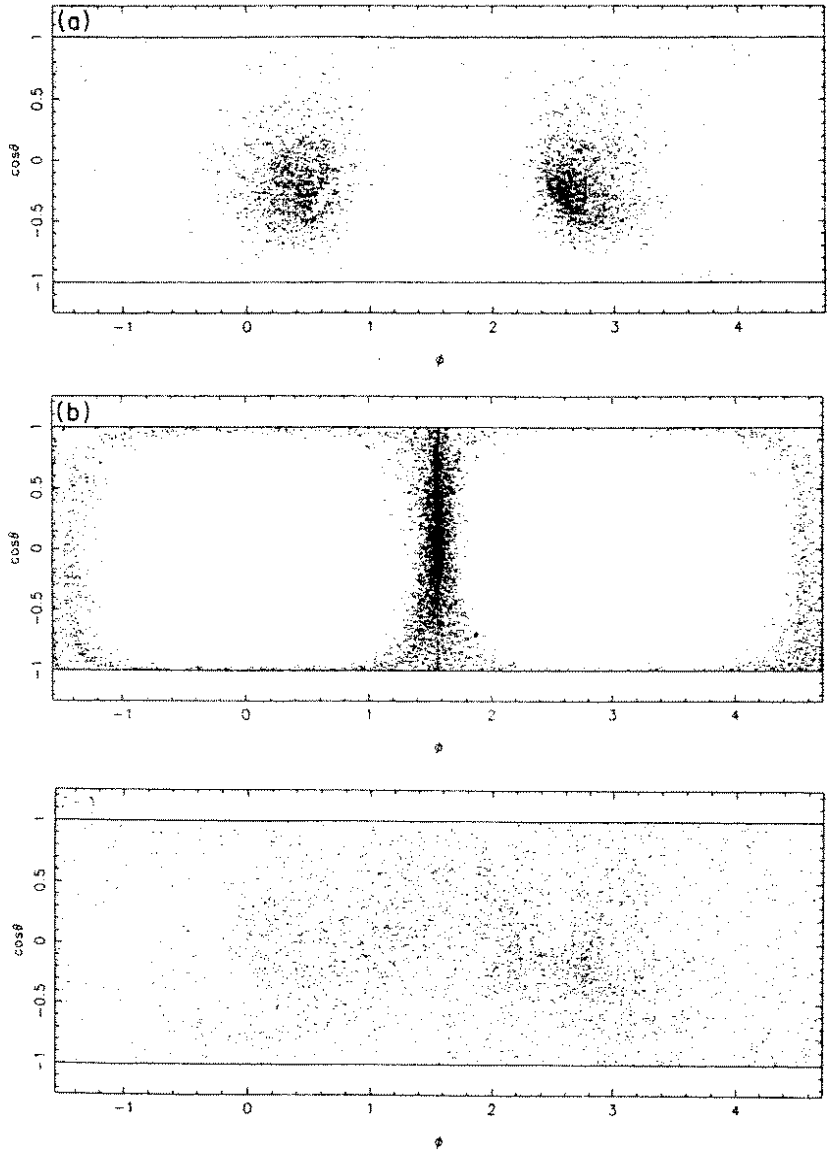

Figure 14: *Stationary probability distributions of the state vector of an atom whose fluorescence is subject to a) homodyne detection where the local oscillator field is in phase with the driving field, b) homodyne detection with a local oscillator $\pi/2$ out of phase wtih the driving field, and c) heterodyne detection. The distributions are approximated by 20.000 points on the Bloch sphere.*

It is possible to associate with the stochastic equations a probability distribution of wave function amplitudes $P(\{c_i\})$, $P(\theta, \phi)$ in this case, and sometimes [50] to identify its equation of motion. The easiest way to obtain the distribution is by means of the Quantum Monte Carlo simulations, and in Fig.14 are shown the results of such simulations, obtained by Wiseman and Milburn [50]. The distributions look very different

for different detection schemes. However, all statements about the system are related to quantum expectation values, which are given by the quantities $\overline{c_i c_j^*}$, and they are identical. Note that these quantities are in fact the ***variances and covariances*** of the distributions $P(\{c_i\})$. The additional information in Fig.14 is not accessible experimentally, and since the master equation is a closed set of equations for these variances and covariances, it is not really needed in calculations either. It may, however, just like the details in the evolution of a single QMC, give us a *picture* of the dynamics of a system.